

1

2 **Responses of atmospheric circulation to sea surface
3 temperature anomalies in the South China Sea**

4

5 **MuPing Zhou, GuiHua Wang**

6 State Key Laboratory of Satellite Ocean Environment Dynamics, Second Institute of
7 Oceanography, State Oceanic Administration, Hangzhou 310012, China

8 Correspondence to: Guihua Wang (gwang@sio.org.cn)

9

1

2 **ABSTRACT**

3 The sea surface temperature (SST) anomalies in the South China Sea (SCS) and their influences
4 on global atmospheric circulation were studied. The results of the simple atmospheric model
5 suggested that the SCS SST anomalies can induce several barotropic wave trains from the SCS to
6 other regions such as North America, high latitudes of the Southern Hemisphere and the
7 Mediterranean. The baroclinic stream function anomalies from the simple model showed an
8 anticyclonic vortex pair in East Asia and southern tropical Indian Ocean and a cyclonic vortex in
9 the North Pacific and the Southwest Pacific. It is suggested that the spatial pattern of SST
10 anomalies in the SCS can affect the magnitude of stream function anomalies, although it cannot
11 affect the spatial pattern of atmospheric circulation.

12

1 **1. Introduction**

2 The South China Sea (SCS, 0-25°N, 100-125°E) is the largest marginal sea in the Northwest
3 Pacific. The sea surface temperature (SST) in the SCS has a significant seasonal cycle. The
4 climatological SSTs in summer (June to August) and winter (December to February) over the
5 SCS are shown in Fig. 1. The SST in summer is mostly above 28°C, with a pronounced cold
6 tongue veering off central Vietnam (Fig. 1a). During winter, the SST is cold in the northwest and
7 warm in the southeast of the SCS (Fig. 1b).

8 The SST in the SCS had a robust warming trend during past several decades (Luo et al.,
9 1986; Fang et al., 2006; Xie et al., 2010; Zhang et al., 2010; Liu and Zhang, 2013). Based on the
10 Optimum Interpolation Sea Surface Temperature (OISST) dataset, Fang et al. (2006) concluded
11 that the SST in the SCS had the positive linear trend of $5^{\circ}\text{C}100\text{a}^{-1}$ during 1993-2003. The
12 summer and winter SST trends in the SCS from 1982 to 2011 are also shown in Fig. 1. Whether
13 in summer or in winter, the SCS warming trend is significant; with $1.64^{\circ}\text{C}100\text{a}^{-1}$ in summer and
14 $2.04^{\circ}\text{C}100\text{a}^{-1}$ in winter. The maximum SST trend can exceed $9.50^{\circ}\text{C}100\text{a}^{-1}$. The averaged SST
15 trend of the SCS is smaller than that reported by Fang et al. (2006), which used the data from
16 1993-2003. During summer, the larger warming is in the western SCS and the smaller in the
17 eastern SCS. While During winter, the larger warming is in the eastern SCS and the smaller in the
18 western SCS. It should be noted that the SCS warming is faster than global average, and the
19 warming is largest between 0-20°N globally.

20 Many studies focused on the effects of the positive SST anomalies in the SCS on
21 precipitation and climate in China (Zhang et al., 2003; Fong et al., 2004; Roxy and Tanimoto,
22 2012). According to Zhang et al. (2003), the positive SST anomaly in summer from the seasonal
23 climatology in the SCS~~the positive SST anomaly in the SCS in summer~~ was followed by
24 anomalous southward wind, and then more moisture was transferred to South China, which
25 resulted in floods in the Yangtze River Valley. Fong et al. (2004) suggested that the SCS surface
26 warming can enhance latent and sensible heat fluxes from the sea surface and result in a cyclonic
27 circulation anomaly in the lower troposphere and an anti-cyclonic circulation anomaly in the
28 upper troposphere, which then affect the climate of South China. Roxy and Tanimoto (2012)
29 pointed out that the positive SST anomalies over the SCS tended to form a favorable condition

1 for convective activity and enhanced the northward propagating precipitation anomalies during
2 the SCS summer monsoon. Other studies showed that the SST anomalies in the SCS can
3 influence SCS monsoon onset (Johnson and Ciesielski, 2002; Ding et al., 2004; Lestari and
4 Iwasaki, 2006) and its variability (Liu and Xie, 1999; Lestari et al., 2011; Roxy and Tanimoto,
5 2012).

6 Teleconnections are well known and well frequently reported (Wallace and Gutzler 1981;
7 Huang, 1984; Nitta, 1986; Nitta, 1987). A local change in the surface boundary condition can
8 have far reaching influences elsewhere. For examples, the diabatic heating anomaly over the
9 central equatorial Pacific during ENSO can excite a stationary barotropic Rossby wave train
10 propagating into extratropical regions. This teleconnection is known as the Pacific-North
11 American (PNA) pattern (Wallace and Gutzler, 1981) in the Northern Hemisphere. Nitta (1987)
12 found an association between abnormal convective activity over the tropical western North
13 Pacific and atmospheric circulation anomalies over the midlatitude of East Asia in summer which
14 named as the Pacific-Japan (PJ) pattern.

15 Previous studies mostly discussed how the SST in the SCS affected the local climate and the
16 teleconnections between the SCS and global atmosphere circulation are not clear. Previous studies
17 mostly discussed how the SST in the SCS affected the local climate. But the extent of impact of
18 the SST anomalies in the SCS is still not known. In this paper, we use a simple atmospheric
19 model to discuss it. The rest of this paper is organized as follows. Section 2 describes the data and
20 model used in this study. The results obtained with the simple atmospheric model are presented in
21 Sect. 3. Summary and discussion are provided in Sect. 4.

22 **2. Data and model**

23 **2.1 Data and method**

24 Two datasets are used in this study. The climatological stream functions are from the National
25 Centers for Environmental Prediction/National Center for Atmospheric Research (NECP/NCAR)
26 reanalysis, which is available on a 2.5° latitude by 2.5° longitude grid (Kalnay et al., 1996).
27 OISST analysis product is from the National Oceanic and Atmospheric Administration (NOAA),
28 which has the spatial resolution of 0.25° latitude by 0.25° longitude (Reynolds et al., 2002). The
29 period of the two datasets used is from 1982 to 2011.

1 The basic mean flows are represented by the stream functions at 250 and 750 hPa from the
2 monthly NCEP/NCAR reanalysis. The stream functions at 750 hPa are constructed by linear
3 interpolation with all standard pressure levels, as 750 hPa is not a standard pressure level. Since
4 the model atmosphere is simplified to two levels (centered at 250 and 750 hPa), the stream
5 functions can be separated into the barotropic and baroclinic components as follows:

6 $\psi_{\text{barotropic}} = 0.5(\psi_{250\text{hPa}} + \psi_{750\text{hPa}})$, (1)

7 $\psi_{\text{baroclinic}} = 0.5(\psi_{250\text{hPa}} - \psi_{750\text{hPa}})$, (2)

8 where ψ stands for stream function.

9 Figure 2 shows the spatial pattern of mean barotropic stream function (a) and baroclinic
10 stream function (b) from 1982 to 2011. Whether barotropic or baroclinic stream function, it was
11 always the westerly in high latitudes. Generally, there were two westerly jet cores in the Northern
12 Hemisphere and consistent westerly in the Southern Hemisphere. In the equatorial and tropical
13 regions, the flows fluctuated due to strong convections.

14 **2.2 Atmospheric model**

15 We use a simple atmospheric model developed recently by Lee et al. (2009) to simulate global
16 atmospheric circulation. This is a steady-state two-level (centered at 250 and 750 hPa)
17 spherical-coordinate primitive equation model, linearized about prescribed background mean
18 flows. The model uses triangular 18 truncations for horizontal grids. The formulation is similar to
19 that of the multi-level linear baroclinic model used by Hoskins and Simmons (1975) and others,
20 but its governing equations are greatly simplified by employing Gill's (1980) simple
21 thermodynamic equation. Detailed description of the simple model can be found in the paper of
22 Lee et al. (2009). This model successfully simulated the local and remote responses of the
23 atmosphere to tropical heating anomalies (Lee et al., 2009; Wang et al., 2010; Zheng et al., 2013).
24 In this study, we use the basic mean flows as the initial conditions and heating in the SCS as the
25 forcing conditions to run this model.

26 **3. Results**

27 **3.1 Influence of SST anomalies in the meridional direction**

1 Two experiments are set up to see how basin-scale SST anomalies affect the atmospheric
2 circulation: 1) uniform heating in the SCS (Case 1) and 2) heating decreased northward in the
3 SCS to consider the differences in solar radiation in the northern and southern SCS (Case 2). To
4 test the effects of seasonal SST anomalies in the SCS, we set up two more experiments: 3)
5 heating pattern similar to the SST winter pattern (Case 3) and 4) heating pattern similar to the
6 SST summer pattern (Case 4) in the SCS. As shown in Fig. 1, the SST in the winter is low in the
7 northwest and high in the southeast SCS, which is used in Case 3, while the summer pronounced
8 cold tongue veering off central Vietnam is included in Case 4. Heating patterns derived from SST
9 anomalies for these four experiments are summarized in Fig. 3. The calculations are listed in
10 Table 1. Note the total heat input is the same for the four experiments to ensure comparability.

11 Figure 4a shows the barotropic stream function anomalies from Case 1. There are three
12 robust waves in the barotropic stream function. The first one is from the SCS to North America
13 through the northwestern Pacific, which is somewhat similar to the classical PNA pattern
14 (Wallace and Gutzler, 1981; Nitta, 1986; Huang, 1984). The second one is from the SCS to high
15 latitudes of the Southern Hemisphere across the equator. As shown by Wang et al. (2010), the
16 background vertical wind shear is important in converting energy from the heating-induced
17 baroclinic flow anomalies into barotropic motions near the heating source. The barotropic
18 anomalies in turn interact with the mean westerly wind to transmit the barotropic signals to the
19 high latitudes of the Southern Hemisphere. Note another small wave train is from the SCS to the
20 Mediterranean. According to the classical theory of energy dispersion (Yeh, 1949) and the great
21 circle theory (Hoskins and Karoly, 1981), disturbances produced by local heating can spread
22 westward.

23 The baroclinic stream function anomalies from the simple model show an anticyclonic
24 vortex pair in East Asia and southern tropic Indian Ocean (Fig. 4b). Accordingly, a cyclonic
25 vortex pair appears in the north and southwest Pacific, quite similar to the Matsuno–Gill model
26 (Gill, 1980) and consistent with the results of Heckley and Gill (1984) and Smagorinsky (1953).
27 The response of atmospheric circulation to the heating anomaly in the SCS suggests that the Gill
28 dynamics is at work.

29 We calculate the seasonal cycle of the air-sea temperature difference (Figures not shown
30 here); it suggests that atmosphere reduces heat loss to the ocean during the boreal winter in the

1 northern SCS and increases heat flux from the ocean during the summer in the northern SCS. It
2 was supported by He and Wu (2013) that the boreal winter SST in the northern SCS are
3 independent from the atmospheric conditions, it gives the opportunity to look in the used
4 observational data sets find support for the described teleconnections. The correlation between
5 the winter SSTA in northern SCS and the barotropic/baroclinic streamfunction are calculated. As
6 shown in Fig. 5, the correlation in Fig. 5a demonstrated two waves: one is from SCS to North
7 America and the other is from SCS to the Southern Hemisphere; the correlation in Fig. 5b
8 showed positive anomalies in East Asia and the Southwest Pacific and negative anomalies in the
9 North Pacific and southern tropical Indian Ocean. These support the described teleconnection
10 between SCS SST and the global atmospheric circulation.

11 The barotropic and baroclinic stream function anomalies for Cases 2-4 are basically the
12 same as for Case 1, which indicates that the positive heating anomalies in the SCS can all induce
13 three waves in the barotropic stream function and two vortex pairs in the baroclinic stream
14 function regardless of the spatial pattern of the heating. The amplitudes are slightly different in
15 the four experiments. For the PNA-like pattern wave train and the Southern Hemisphere wave
16 train, the barotropic stream functions in Cases 1 and 4 are weaker than those in Cases 2 and 3 in
17 the anticyclonic anomalies, but they are stronger than those in Cases 2 and 3 in the cyclonic
18 anomalies (Fig. 5a6a). Conversely, the baroclinic stream functions of Cases 1 and 4 are weaker
19 than those in Cases 2 and 3 in the cyclonic anomalies, but are stronger than those in Cases 2 and
20 3 in the anticyclonic anomalies (Fig. 5b6b). The differences among the four cases suggest that the
21 spatial pattern of SST anomalies can affect the magnitude of stream functions, although it cannot
22 affect the spatial pattern of atmospheric circulation. The role of asymmetric heating in
23 influencing atmosphere circulation also can be seen in many literatures such as Fu et al. (1980)
24 and Dunkerton (1989). The results support that the waves n=1, 2 are distinctly controlled by the
25 asymmetric heating sources revealed by Fu et al. (1980).

26 3.2 Influence of SST anomalies in the zonal direction

27 To test the effects of the SST warming differences in the zonal direction on atmospheric
28 circulation, To test the effects of the SST warming patterns in the SCS on atmospheric circulation
29 in the zonal direction, we carry out two more experiments, using summer and winter SST

1 warming trend heating patterns, respectively. Figure 6-7 shows the stream function anomalies of
2 the barotropic and baroclinic components for Cases 5 and 6, which are also summarized in Table
3 1. Note the heating pattern in the two experiments is similar to the warming trend pattern, while
4 the total heat input in these two cases is the same as in Cases 1-4 to ensure comparability.

5 The spatial patterns of the stream function anomalies for Cases 5 and 6 are also quite similar
6 to those in Case 1 for both barotropic or baroclinic components. For the PNA-like pattern wave
7 train or the Southern Hemisphere wave train, the barotropic stream function in Case 5 is weaker
8 than that in Case 6 in the cyclonic anomalies, but is stronger than that in Case 6 in the
9 anticyclonic anomalies (Fig. 6a7a). Conversely, the baroclinic stream function in Case 5 is
10 weaker than that in Case 6 in the anticyclonic anomalies, but is stronger than that in Case 6 in the
11 cyclonic anomalies (Fig. 6b7b). As shown in Fig. 1, the larger warming trend is in the western
12 SCS for the summer but in the eastern SCS for the winter. The difference between Cases 5 and 6
13 suggests that the larger warming trend in the western (eastern) SCS heating pattern can weaken
14 (strengthen) the cyclonic anomalies and strengthen (weaken) the anticyclonic anomalies in the
15 barotropic component. On the contrary, the larger warming trend in the western (eastern) SCS
16 heating pattern can strengthen (weaken) cyclonic anomalies and weaken (strengthen) the
17 anticyclonic anomalies in the baroclinic component. It also suggests that the spatial pattern of
18 SST trend can affect the magnitude of stream functions, although it cannot affect the spatial
19 pattern of atmospheric circulation.

20 4. Summary and discussion

21 In this study, the influences of SST anomalies in the SCS on global atmospheric circulation were
22 studied. The results of the simple atmospheric model suggested that the SCS heating can induce a
23 barotropic wave train from the SCS to the Northwest Pacific and North America, which is
24 somewhat similar to the classical PNA pattern. Simultaneously, the SCS heating can induce a
25 barotropic wave train from the SCS to high latitudes of the Southern Hemisphere. In particular,
26 we noticed a weak barotropic wave train from the western SCS to the Mediterranean. The
27 baroclinic stream function anomalies from the simple model showed an anticyclonic vortex pair
28 in East Asia and the southern tropic Indian Ocean and a cyclonic vortex in the North Pacific and
29 the Southwest Pacific. The stream function anomalies of the barotropic and baroclinic

1 components for all six cases are basically the same, with slight differences in amplitude. It
2 suggests that the spatial pattern of heating can cause some differences in magnitude, but not in
3 circulation patterns. Our findings in this study may be important for the regional and global
4 climate research. For example, we calculate the correlation between the northern SCS SSTA and
5 the rainfall. The correlation pattern is quiet similar to Fig. 4a, which also showed two waves: one
6 is from SCS to North America and the other is from SCS to the Southern Hemisphere (Figures
7 not shown here), thus this study may help to forecast climate-related events like rainfall in the
8 North America based on the SCS SST anomalies. For example, we may forecast climate related
9 events based on the SCS SST anomalies.

10 Note heating in the atmosphere is not necessarily collocated to SST warming in observations.
11 In some cases, the SST warming results from descending in the atmosphere and thus it may not
12 be a cause of heating. For example, He and Wu (2013) indicated that the SST anomalies in the
13 South China Sea are mostly response to the atmospheric changes except for boreal winter in the
14 northern South China Sea. We completely ignore the situation and simply consider that the SST
15 anomalies can induce heat to the atmosphere. Thus a more complete atmospheric general
16 circulation model is necessary to confirm these findings.

17

18 **Acknowledgments.** We thank Dr. Sang-Ki Lee and Dr. Chunzai Wang for sharing the model code
19 and helping to run the model. This study was supported by the National Basic Research Program
20 of China and the National Natural Science Foundation of China.

1

2 **References**

3 Ding, Y. H., Li, C. Y., and Liu, Y. J.: Overview of the South China Sea monsoon experiment. *Adv.*
4 *Atmos. Sci.*, 21:3, 343-360, doi: 10.1007/BF02915563, 2004.

5 Dunkerton, T. J.: Nonlinear Hadley circulation driven by asymmetric differential heating [J]. *J.*
6 *Atmos. Sci.*, 46(7): 956-974, 1989.

7 Fang, G. H. Wei, Chen, Z., Wang, Y., Wang, X., and Li, C.: Trends and interannual variability of
8 the South China Sea surface winds, surface height, and surface temperature in the recent
9 decade. *J. Geophys. Res.*, 111, C11S16, doi: 10.1029/2005JC003276, 2006.

10 Fong, S. K., Wu, C. S., Wang, A. Y., Ku, C. M., Hao, I. P., and Tong, T. N.: A numerical study of
11 the effects of South China Sea SST anomalies on the climate in South China. *Journal of*
12 *Tropical Meteorology*, 20:1, 32-38 (in Chinese), 2004.

13 Fu, K. Z., Wu, H. D., Fang, X. F., Wang, Y. K.: Asymmetric heating effects on the general
14 circulation of atmosphere. *Acta Meteorologica Sinica*, 38:3, 205-218(in Chinese), 1980.

15 Gill, A. E.: Some simple solutions for heat-induced tropical circulation. *Quart. J. Roy. Meteor.*
16 *Soc.*, 106, 447–462, doi: 10.1002/qj.49710644905, 1980.

17 He, Z. Q., and Wu, R. G.: Seasonality of interannual atmosphere–ocean interaction in the South
18 China Sea. *J. Oceanogr.*, 69(6), 699-712. doi: 10.1007/s10872-013-0201-9, 2013.

19 Heckley, W. A., and Gill, A. E.: Some simple analytical solutions to the problem of forced
20 equatorial long waves. *Quart. J. Roy. Meteor. Soc.*, 110(463), 203-217. DOI:
21 10.1002/qj.49711046314, 1984

22 Hoskins, B. J., and Simmons, A. J.: A multi-layer spectral model and the semi-implicit method.
23 *Quart. J. Roy. Meteor. Soc.*, 101, 637–655, doi: 10.1002/qj.49710142918, 1975.

24 Hoskins, J. Brian, and Karoly, D. J.: The Steady Linear Response of a Spherical Atmosphere to
25 Thermal and Orographic Forcing. *J. Atmos. Sci.*, 38, 1179–1196, doi:
26 [http://dx.doi.org/10.1175/1520-0469\(1981\)038<1179:TSLROA>2.0.CO;2](http://dx.doi.org/10.1175/1520-0469(1981)038<1179:TSLROA>2.0.CO;2), 1981.

27 Huang, R. H.: The characteristics of the forced stationary planetary wave propagations in summer
28 Northern Hemisphere. *Adv. Atmos. Sci.*, 1:1, 84-94, doi: 10.1007/BF03187619, 1984.

29 Johnson, R. H. and Ciesielski, P. E.: Characteristics of the 1998 summer monsoon onset over the

1 northern South China Sea, *J. Meteorol. Soc. Jpn. Ser. II*, 80:4, 561-578, doi:
2 <http://dx.doi.org/10.2151/jmsj.80.561>, 2002.

3 Kalnay, E., Kanamitsu, M., Kistler, R., Collins, W., Deaven, D., Gandin, L., Iredell, M., Saha, S.,
4 White, G., Woollen, J., Zhu, Y., Leetmaa, A., Reynolds, B., Chelliah, M., Ebisuzaki, W.,
5 Higgins, W., Janowiak, J., Mo, K. C., Ropelewski, C., Wang, J., Jenne, R., and Joseph, D.:
6 The NCEP/NCAR 40-Year Reanalysis Project. *Bull. Amer. Meteor. Soc.*, 77, 437–471, doi:
7 [http://dx.doi.org/10.1175/1520-0477\(1996\)077<0437:TNYRP>2.0.CO;2](http://dx.doi.org/10.1175/1520-0477(1996)077<0437:TNYRP>2.0.CO;2), 1996.

8 Lee, S. K., Wang, C. Z., and Mapes, B. E.: A Simple Atmospheric Model of the Local and
9 Teleconnection Responses to Tropical Heating Anomalies. *J. Climate*, 22, 272–284, doi:
10 <http://dx.doi.org/10.1175/2008JCLI2303.1>, 2009.

11 Lestari, R. K., Watanabe, M., and Kimoto, M.: Role of air-sea coupling in the interannual
12 variability of the South China Sea summer monsoon. *J. Meteorol. Soc. Jpn. Ser. II*, 89,
13 283-290, doi: <http://dx.doi.org/10.2151/jmsj.2011-A18>, 2011.

14 Lestari, R. K., and Iwasaki, T.: A GCM study on the roles of the seasonal marches of the SST and
15 land-sea thermal contrast in the onset of the Asian summer monsoon. *J. Meteorol. Soc. Jpn. Ser. II*, 84(1), 69-83, 2006.

17 Liu, W. T., and Xie, X.: Space-based observations of the seasonal changes of South Asian
18 monsoons and oceanic response, *Geophys. Res. Lett.*, 26, 1473–1476, doi:
19 [10.1029/2003JC001867](https://doi.org/10.1029/2003JC001867), 1999.

20 Liu, Q., and Zhang, Q.: Analysis on long-term change of sea surface temperature in the China
21 Seas. *J. Ocean Univ. China*, 12:2, 295-300. doi: [10.1007/s11802-013-2172-2](https://doi.org/10.1007/s11802-013-2172-2), 2013.

22 Luo, S. H., and Jin, Z. H.: Statistical analyses for sea surface temperature over the South China
23 Sea, behavior of subtropical high over the west pacific and monthly mean rainfall over the
24 Chang Jiang middle and lower reaches. *Journal of Atmospheric Sciences*. 10.4, 409-418 (in
25 Chinese), 2006.

26 Nitta, T.: Convective activities in the tropical western pacific and their impact on the northern
27 hemisphere circulation. *J. Meteorol. Soc. Jpn.*, 65, 373-390, 1987.

28 Nitta, T.: Long-term variations of cloud amount in the western Pacific region. *J. Meteorol. Soc.*
29 *Jpn.*, 64:3, 373-390, 1986.

30 Reynolds, R. W., Rayner, N. A., Smith, T. M., Stokes, D. C., and Wang, W. Q.: An improved in

1 situ and satellite SST analysis for climate, *J. Clim.*, 15:13, 1609–1625, doi:
2 [http://dx.doi.org/10.1175/1520-0442\(2002\)015<1609:AIISAS>2.0.CO;2](http://dx.doi.org/10.1175/1520-0442(2002)015<1609:AIISAS>2.0.CO;2), 2002.

3 Roxy, M., and Tanimoto, Y.: Influence of sea surface temperature on the intraseasonal variability
4 of the South China Sea summer monsoon. *Clim. Dyn.*, 39:5, 1209-1218, doi:
5 10.1007/s00382-011-1118-x, 2012.

6 Smagorinsky, J.: The dynamical influence of large-scale heat sources and sinks on the
7 quasi-stationary mean motions of the atmosphere. *Q. J. R. Meteorol. Soc.*, 79, 342–366. doi:
8 10.1002/qj.49707934103, 1953.

9 Wallace, J. M., and Gutzler, D. S.: Teleconnections in the geopotential height field during the
10 Northern Hemisphere winter. *Mon. Wea. Rev.*, 109, 784–812, doi:
11 [http://dx.doi.org/10.1175/1520-0493\(1981\)109<0784:TITGHF>2.0.CO;2](http://dx.doi.org/10.1175/1520-0493(1981)109<0784:TITGHF>2.0.CO;2), 1981.

12 Wang, C. Z., Lee, S. K., Mechoso, C. R.: Interhemispheric Influence of the Atlantic Warm Pool
13 on the Southeastern Pacific. *J. Climate*, 23:2, 404-418, doi: <http://dx.doi.org/10.1175/2009JCLI3127.1>, 2010.

14 Xie, S. P., Deser, C., Vecchi, A. G., Ma, J., Tend, H., and Wittenberg, A. T.: Global warming
15 pattern formation: sea surface temperature and rainfall. *J. Climate*, 23: 966-986, doi:
16 <http://dx.doi.org/10.1175/2009JCLI3329.1>, 2010.

17 Yeh, T.: ON ENERGY DISPERSION IN THE ATMOSPHERE. *J. Meteor.*, 6, 1–16, doi:
18 [http://dx.doi.org/10.1175/1520-0469\(1949\)006<0001:OEDITA>2.0.CO;2](http://dx.doi.org/10.1175/1520-0469(1949)006<0001:OEDITA>2.0.CO;2), 1949.

19 Zhang Q., Liu, P., and Wu, G. X.: The relationship between the flood and drought over the lower
20 reach of the Yangtze River Valley and the SST over the Indian Ocean and the South China
21 Sea. *Journal of Atmospheric Sciences*, 27 (6), 992-1006 (in Chinese) , 2003.

22 Zhang, L. P., Wu, L. X., Lin, X. P., and Wu, D. X.: Modes and mechanisms of sea surface
23 temperature low-frequency variations over the coastal China seas. *J. Geophys. Res.*, 115,
24 C08031, doi: 10.1029/2009JC006025, 2010.

25 Zheng, J., Liu, Q. Y., Wang, C. Z., and Zheng, X. T.: Impact of heating anomalies associated with
26 rainfall variations over the indo-western Pacific on Asian atmospheric circulation in winter.
27 *Clim. Dyn.*, 40, 2023-2033, doi: 10.1007/s00382-012-1478-x, 2013.

28

Table 1. The heat forcing Q at each grid for Cases 1-6.

| Exp. | Heat forcing in the SCS | Description |
|--------|--|--|
| Case 1 | $Q(i, j)=Q_0^*$ | Uniform heating |
| Case 2 | $Q(i, j)=Q_0 \cdot (25-\text{lat}(i, j))/12.5$ | Heating less in the north |
| Case 3 | $Q(i, j)=Q_0 \cdot ((25-\text{lat}(i, j))+(125-\text{lon}(i, j)))/25$ | Similar to SST winter pattern |
| Case 4 | $Q(i, j)=Q_0 \cdot ((12.5-\text{lat}(i, j))^2/10+\text{lon}(i, j)-100)/18.125$ | Similar to SST summer pattern |
| Case 5 | $Q(i, j)=Q_0 \cdot \text{summer SST trends pattern}/1.64$ | summer SST trends pattern |
| Case 6 | $Q(i, j)=Q_0 \cdot \text{winter SST trends pattern}/2.04$ | winter SST trends pattern |
| | | $^*Q_0=1.16 \times 10^{-2} \text{W kg}^{-1} (1 \text{ }^{\circ}\text{C day}^{-1})$ |

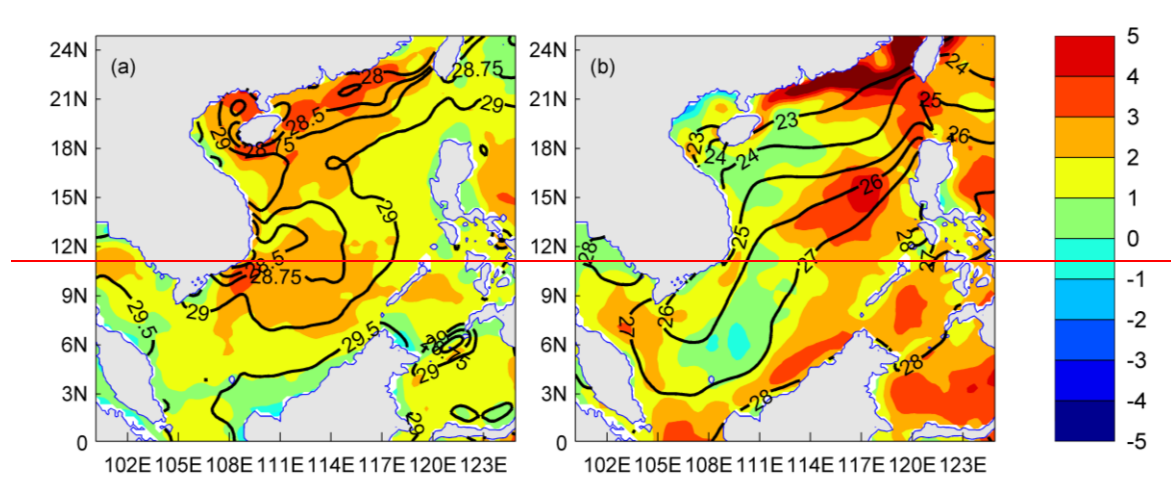
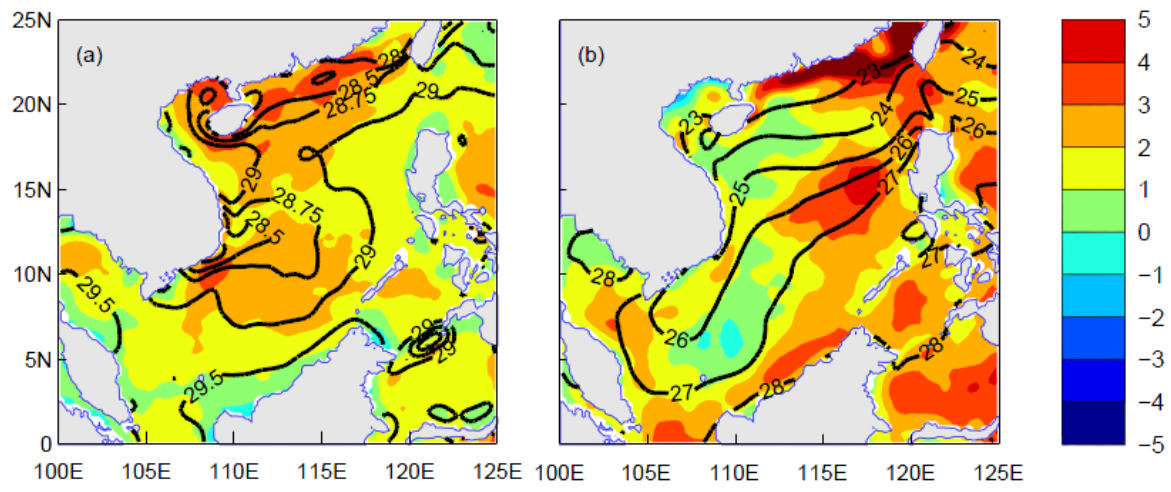


Figure 1. (a) Summer- and (b) winter-mean SST (contours; units: $^{\circ}\text{C}$) and SST trends (color shading; units: $^{\circ}\text{C}100\text{a}^{-1}$) in the SCS from 1982 to 2011.

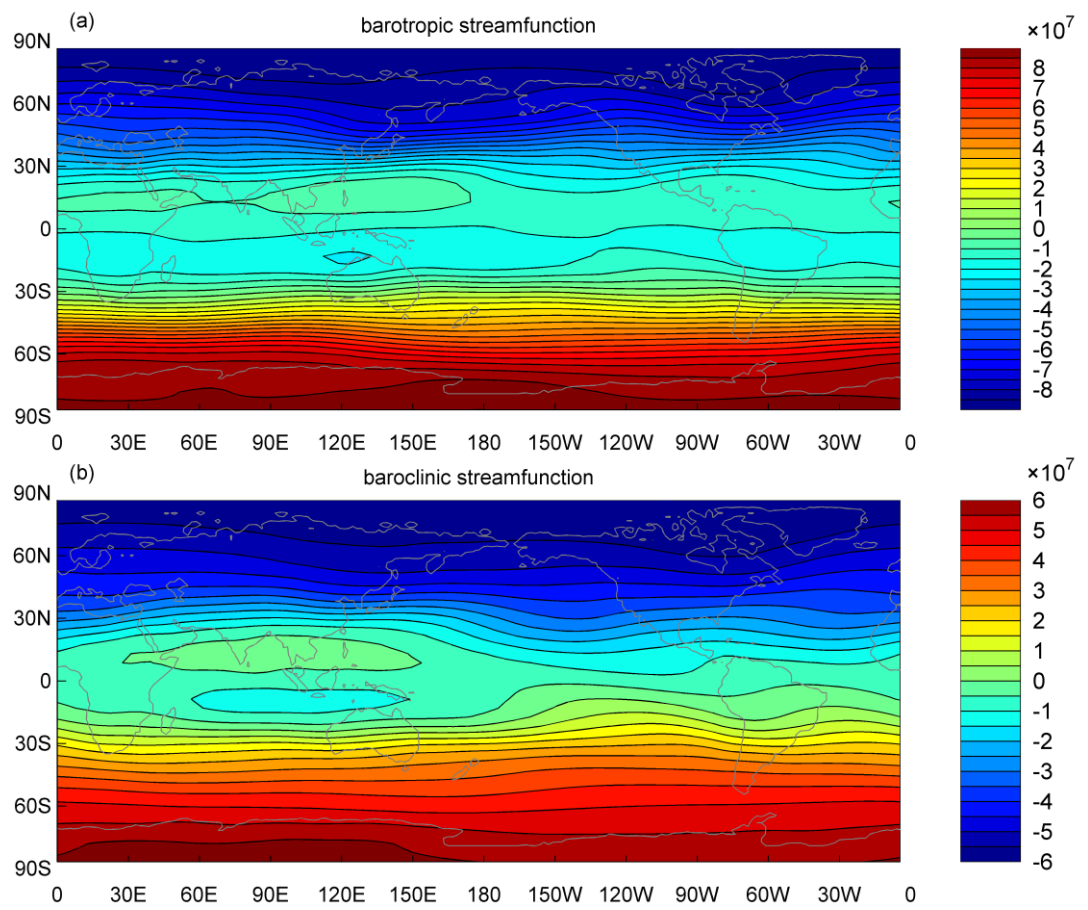


Figure 2. (a) Barotropic and (b) baroclinic stream functions in climatology. The contour interval is $5.0 \times 10^6 \text{ m}^2 \text{ s}^{-1}$.

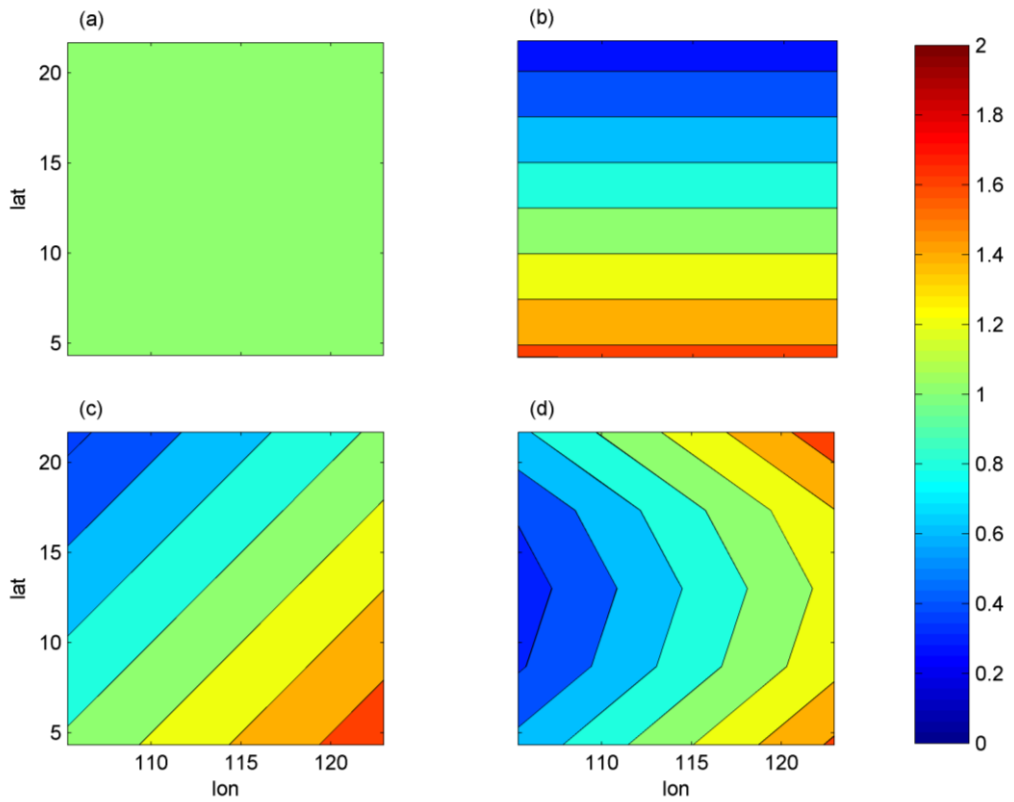


Figure 3. Spatial patterns of heat forcing Q for case 1-4 (a-d, units: Q_0).

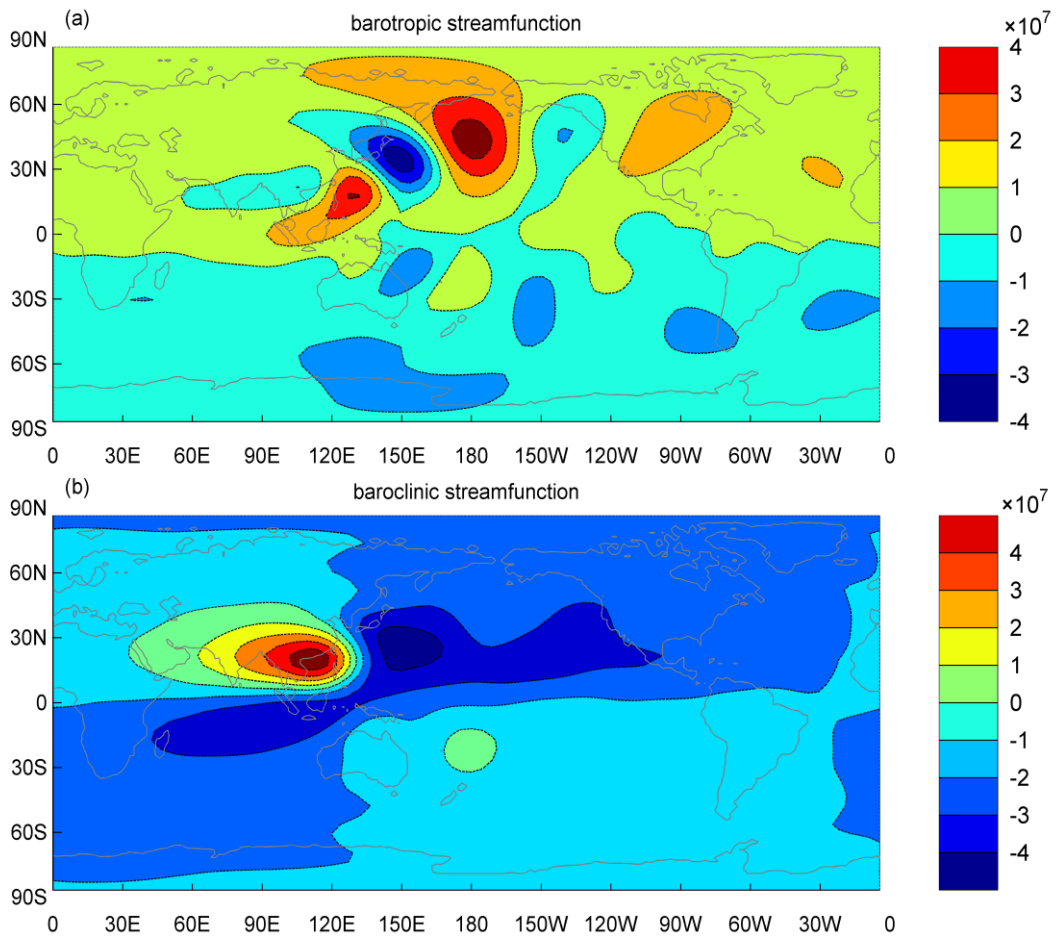


Figure 4. Barotropic (a) and baroclinic (b) stream function anomalies for Case 1. The contour interval is $1 \times 10^6 \text{ m}^2 \text{ s}^{-1}$.

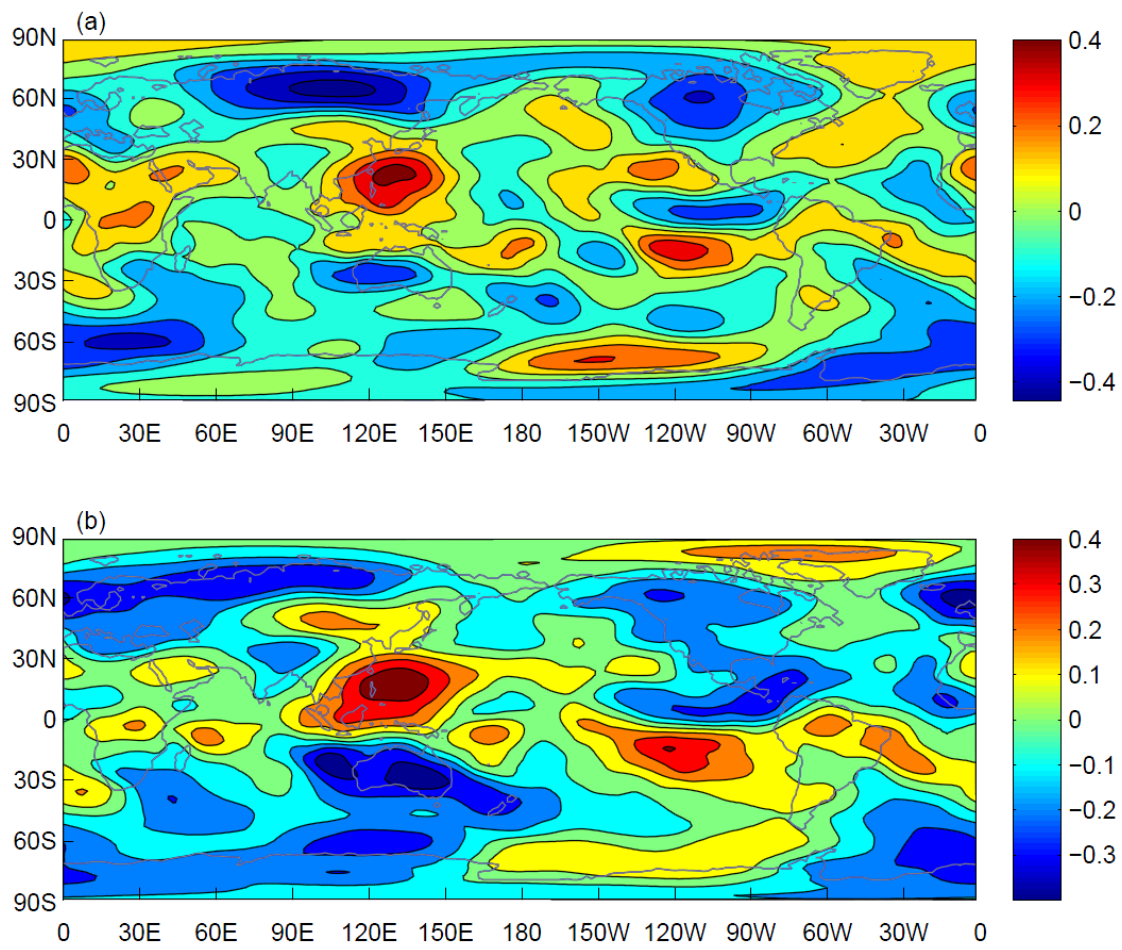


Figure 5. Lag correlation maps (lag day=15 day) of the northern SCS (12–23°N, 110–121°E) SSTA in the winter (October 2003 to March 2004) with global barotropic stream function (a) and baroclinic stream function (b).

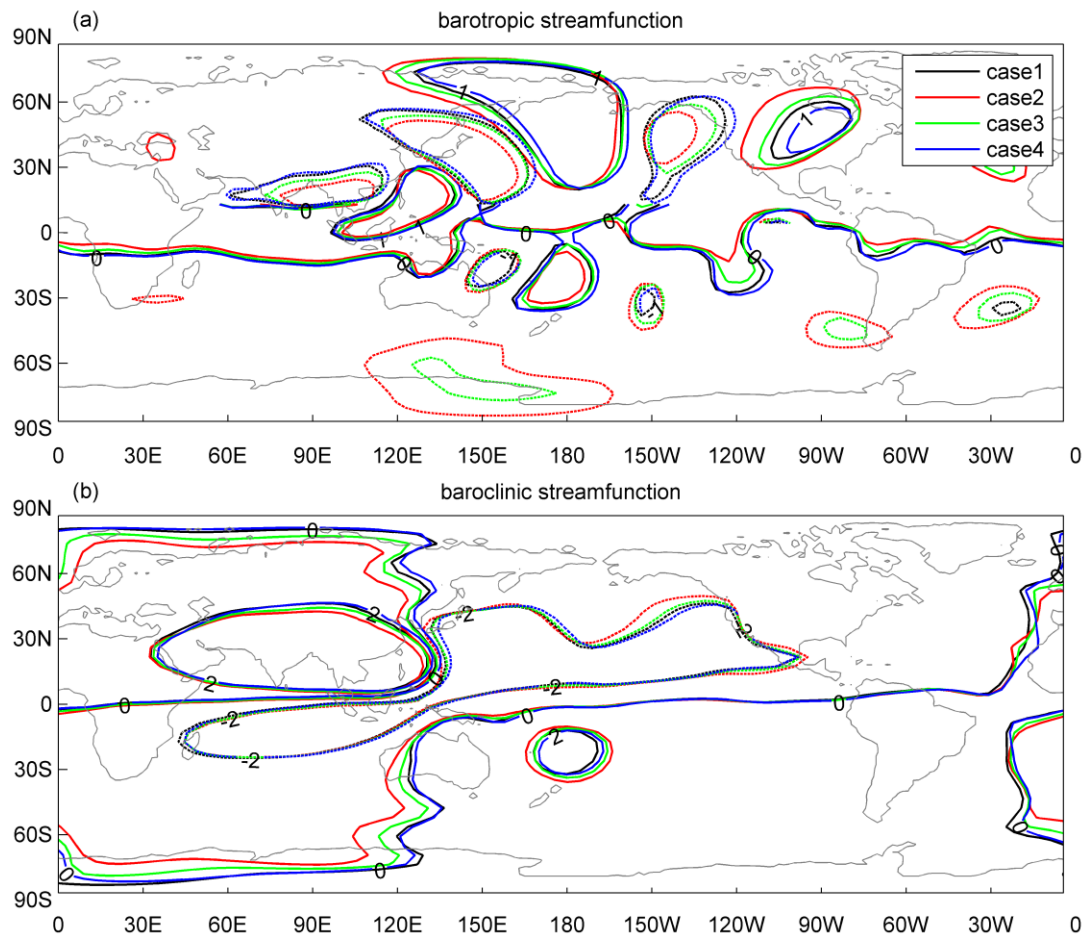


Figure 56. (a) Barotropic and (b) baroclinic stream function anomalies (units: $10^6 \text{m}^2 \text{s}^{-1}$) for Cases 1-4 (the black, red, green, and blue contours are stream function anomalies for Cases 1, 2, 3, and 4, respectively). The contour interval is $2 \times 10^6 \text{m}^2 \text{s}^{-1}$.

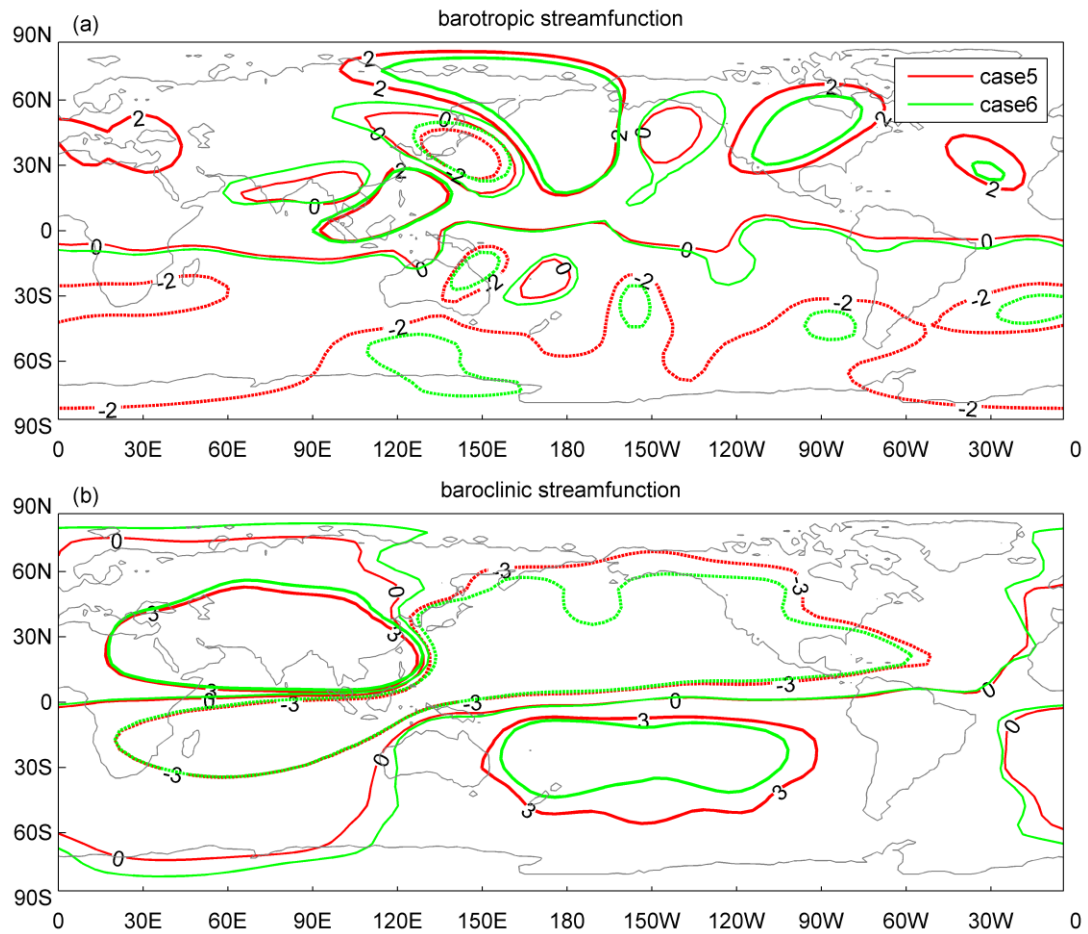


Figure 67. (a) Barotropic and (b) baroclinic stream function anomalies ($10^6 \text{ m}^2 \text{ s}^{-1}$) for Cases 5 (red contours) and 6 (green contours). The contour interval is $2 \times 10^6 \text{ m}^2 \text{ s}^{-1}$ in the top panel and $3 \times 10^6 \text{ m}^2 \text{ s}^{-1}$ in the bottom panel.